JOURNAL OF NANO- AND ELECTRONIC PHYSICS
Vol. **6** No 1, 01007(6pp) (2014)

ЖУРНАЛ НАНО- ТА ЕЛЕКТРОННОЇ ФІЗИКИ
Том **6** № 1, 01007(6cc) (2014)

Effect of Composition on Optical and Thermoelectric Properties of Microstructured *p*-type $(Bi_2Te_3)_x(Sb_2Te_3)_{1-x}$ Alloys

K. Sharma[1,*], M. Lal[2], V.K. Gumber[3], A. Kumar[1], N. Chaudary[1], N. Goyal[1,†]

[1] *Department of Physics, Panjab University, 160014 Chandigarh, India*
[2] *Goswami Ganesh Dutta Sanatan Dharam College, 160030 Chandigarh, India*
[3] *National Physical Laboratory, Council of Scientific and Industrial Research, 110012 New Delhi, India*

(Received 18 December 2013; revised manuscript received 20 January 2014; published online 06 April 2014)

Semiconducting $(Bi_2Te_3)_x(Sb_2Te_3)_{1-x}$ alloys are among the best thermoelectric materials available today near room temperature. This property is largely attributed to compositional variations, resulting in improved figure of merit. Considering this, present study aimed at characterizing the optical and thermoelectric properties of microstructured p-type $(Bi_2Te_3)_x(Sb_2Te_3)_{1-x}$ alloys for enhanced thermoelectric efficiency. High performance microstructured p-type $(Bi_2Te_3)_x(Sb_2Te_3)_{1-x}$ alloys were prepared by melting technique. The phase, optical band gap, microstructure, carrier type concentration and thermoelectric properties of the prepared alloys were systematically investigated by X-ray diffraction, Fourier transform infrared spectroscopy, scanning electron microscopy, hot probe p-n type tester, four-probe method, κ-probe method and Seebeck coefficient measurement system. The electrical conductivity and Seebeck coefficient were measured in the temperature range 298-473 K to elucidate the Sb content effect on the thermoelectric properties of the p-type $(Bi_2Te_3)_x(Sb_2Te_3)_{1-x}$ alloys. The optical band gap decreased with increasing Sb content. Also, with the increase of Sb content, the electrical conductivity increased substantially, the thermal conductivity increased significantly and the Seebeck coefficient decreased marginally, which lead to a great improvement in the thermoelectric figure of merit. The maximum power factor of $3.2 \times 10^{-3}\,Wm^{-1}K^{-2}$ and figure of merit of 0.72 were obtained at 300 K for the composition of 15 %Bi_2Te_3-85 %Sb_2Te_3.

Keywords: Optical band gap, Microstructure, Electrical, Thermoelectric properties.

PACS numbers: 78.20. – e, 33.20.Ea, 72.20.Jv, 72.20.Pa, 84.32.Ff, 61.66.Dk

1. INTRODUCTION

Thermoelectric (TE) materials have widely employed in power generator [1], Peltier cooler [2] and novel type sensors, including: TE hydrogen sensor [3], TE anemometer [4], TE wear sensor [5], TE humidity sensor [6], TE infrared sensor [7-8] and so on. The efficiency of TE materials is generally represented by a figure of merit, $Z = \sigma\alpha^2/\kappa$, or the dimensionless, ZT, where α is the Seebeck coefficient, σ is the electrical conductivity, κ is the thermal conductivity of the material and T is the absolute temperature. These materials have potential to act as thermoelectric devices at room temperature since they have high Seebeck coefficient. A good TE material should have a high electrical conductivity like a crystalline material and a low thermal conductivity like a glass, as suggested by Slack with the concept of "phonon-glass / electron-crystal"s PGEC model [9-14]. The basic crystal structures of these materials ensure the good electrical properties and the spacious voids or cages in the lattice structures reduce the thermal conductivity of the materials by the strong phonon scattering [15-16]. Many bismuth and antimony based thermoelectric materials including n-type $Bi_2(Te, Se)_3$ and p-type Sb_2Te_3 have been studied and Figure of merit of the thermoelectric materials can be improved by an increase of Seebeck coefficient and electrical conductivity and decrease of thermal conductivity. The highest figure of merit even observed for TE materials has been reported by Venkatasubramanian and co-workers with $ZT = 2.4$ at room temperature for *p*-type Bi_2Te_3 / Sb_2Te_3 super lattice thin film [17]. Though all new electric materials have $ZT < 1$, theoretical results of Hicks *et al.* predicted that the thermoelectric devices fabricated as 2-D quantum well or 1-D quantum wires could have $ZT > 3$ [18]. Significant progress has been made in recent years and it indicates that the low-dimensional materials have high thermoelectric conversion efficiency [19-21].

Thermoelectric properties for Bi-Te based alloys were considerably affected by preparation methods. A ZT value of 1.56 at 300 K was obtained by melting spinning *p*-type $Bi_{0.52}Sb_{1.48}Te_3$ bulk material combined with a spark plasma sintering process [22]. Bi-Sb-Te materials were prepared by zone melting technique and maximum ZT of 1.14 was obtained at about 350 K for composition of 24 %Bi_2Te_3-76 %Sb_2Te_3 with 3 wt % excess Te [23]. The ZT value could be modified by adjusting the ratio of Bi and Sb due to change of carrier concentration and thermal conductivity. Chan et al. [24] prepared $(Bi_xSb_{1-x})_2Te_3$ materials in the composition range of $x = 0.15$-0.25 and found that the $(Bi_{0.25}Sb_{0.75})_2Te_3$ has maximum ZT of 0.588. Li et al. [25] prepared $(Bi_2Te_3)_x(Sb_2Te_3)_{1-x}$ materials in composition range of $x = 0.16$-0.24 by the fusion method together with spark plasma sintering and obtained ZT value of 1.33 at 398 K and 1.05 at 300 K for the composition of 20 % Bi_2Te_3 – 80 % Sb_2Te_3 with 3 wt % excess Te. From the literature survey it is clear that the value of ZT depends upon composition as well as the preparation method.

* kanchan785@gmail.com
† ngoyal@pu.ac.in

In the present work, $(Bi_2Te_3)_x(Sb_2Te_3)_{1-x}$ thermoelectric materials in the composition range of $x = 0.15$-0.30 have been prepared and their optical and thermoelectric properties have been studied. The efforts have been made to synthesize good quality of $(Bi_2Te_3)_x(Sb_2Te_3)_{1-x}$ ($x = 0.15$, 0.2, 0.25 and 0.3) materials by melting method which is very easy, economical and reliable in terms of repeatability.

2. EXPERIMENTAL DETIALS

A High purity 99.999 % Bi, Sb and Te granules were weighted according to the formula of $(Bi_2Te_3)_x(Sb_2Te_3)_{1-x}$ ($x = 0.15$, 0.2, 0.25 and 0.3). The powder mixture was loaded into quartz ampoule and sealed under vacuum at 10^{-4} Pa. The sealed quartz ampoule was loaded in a furnace and heated to 800 °C for 15 hours to ensure the composition homogeneity and quenched to room temperature. The ingot was crushed, separated, grounded and characterized.

The crystal phase of the sample was studied by Philips PW-1710 X-ray diffartometer using CuK_α radiation. The FTIR spectra were recorded using Perkin Elmer PE-RX 1 FTIR spectrophotometer. The optical transmission spectra for all four alloys were measured in the spectral range of 2500 nm to 25000 nm. The Scanning electron microscopy was done for structural information.

The thermoelectric properties were measured using specimens having 12 mm diameter and 2 mm thickness. The electrical conductivity (σ) was measured by using four probe method. At room temperature the thermal conductivity was measuredby κ probe- method. In this method the mica, glass, Teflon, Bakelite and silver which have low value of thermal conductivity were used as the reference samples. The carrier type concentration was measured by hot probe p-n type tester. The Seebeck coefficient (α) was obtained by measuring voltage between both ends of the specimens after applying constant temperature difference between both ends in the temperature range 298K-470 K. A T-type differential thermocouple was attached to fluke thermometer to read the temperature difference of the sample. The Seebeck measurement was performed under vacuum.

3. RESULT AND DISCUSSION

The XRD measurement was carried out on the powder sample by using Cu K_α line radiation with wavelength 1.54 Å and shown in Fig. 1. The XRD patterns verify that all samples were in single phase, consist of very sharp well resolved peaks and having rhombohedral crystal structure. In all cases, the peaks centered at $2\theta = 28.33$ ° having highest intensity for the reflection at (015) plane.

The FTIR spectra of all alloys are shown in Fig. 2. In all cases, the peaks occurred at 3415 cm^{-1} correspond to the – OH group of H_2O, at 2925 cm^{-1} and 2362 cm^{-1} due to C – H bond of the $-CH_3-$ and $-CH_2-$ groups. When $x = 0.2$, 0.25 and 0.3, the peaks occurred at 1645 cm^{-1} due to C = O stretching mode, at around 1423 cm^{-1} due to C – H bond of the $-CH_3-$ and $-CH_2-$ groups, at 1043 cm^{-1} due to Bi, at around 675 cm^{-1} due to Sb.

The optical transmission spectra were measured in the spectral range of 2500 nm to 25000 nm. From the transmission data, the value of absorption coefficient (α) was calculated in the region of strong absorption using the relation:

$$\alpha = \log 100/T \quad (1)$$

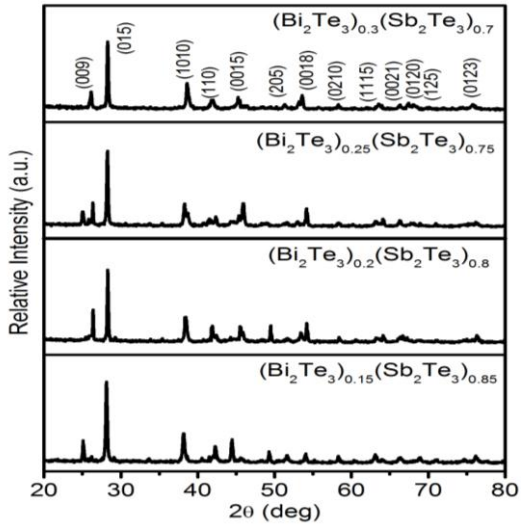

Fig. 1 – XRD 2θ patterns of $(Bi_2Te_3)_x(Sb_2Te_3)_{1-x}$ ($x = 0.15$, 0.2, 0.25 and 0.3) alloys

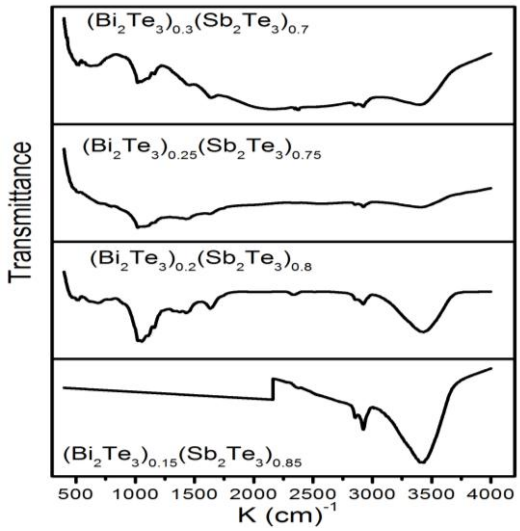

Fig. 2 – FT-IR spectra of $(Bi_2Te_3)_x(Sb_2Te_3)_{1-x}$ ($x = 0.15$, 0.2, 0.25 and 0.3) alloys

The analysis of absorption coefficient was carried out to obtain the optical band gap (E_g). The optical band gap was determined from absorption coefficient data as a function of ($h\nu$) by using Tauc relation [26].

$$\alpha = A(h\nu - E_g)^n/h\nu \quad (2)$$

where A is a constant, E_g is the optical band gap of the material and the exponent n depends on the type of transition and have values 1/2, 2, 3/2 and 3 corresponding to the allowed direct, allowed indirect, forbidden direct and forbidden indirect transitions, respectively. The values of optical band gap (E_g) was calculated by extrapolating the straight line portion of $(\alpha h\nu)^{1/n}$ vs. $h\nu$

by taking $n = 0.5$ as shown in Fig. 3. The calculated values of E_g for all samples are given in Table 1. It is evident from Table 1, optical band gap (E_g) decreased with increase of the Sb content. Hence, the observed band gap shrinkage is dependent on the carrier concentration thereby resulting in narrowing band gap effect.

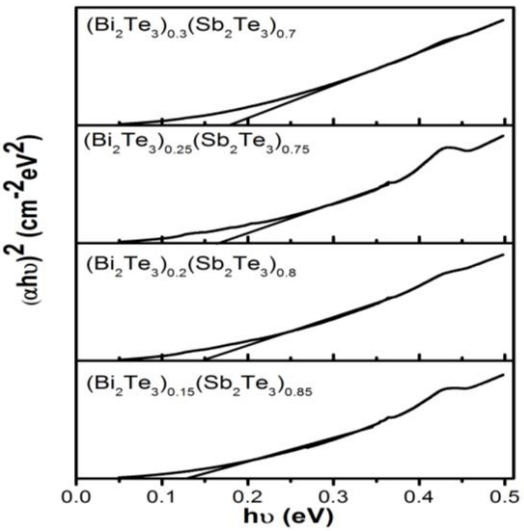

Fig. 3 – Optical band gap of $(Bi_2Te_3)_x(Sb_2Te_3)_{1-x}$ ($x = 0.15$, 0.2, 0.25 and 0.3) alloys

Table 1 – Optical band gap of $(Bi_2Te_3)_x(Sb_2Te_3)_{1-x}$ ($x = 0.15$, 0.2, 0.25 and 0.3)

Material	Optical band gap(eV)
$(Bi_2Te_3)_{0.3}(Sb_2Te_3)_{0.7}$	0.18
$(Bi_2Te_3)_{0.25}(Sb_2Te_3)_{0.75}$	0.17
$(Bi_2Te_3)_{0.2}(Sb_2Te_3)_{0.8}$	0.15
$(Bi_2Te_3)_{0.15}(Sb_2Te_3)_{0.85}$	0.13

The SEM micrographs of fracture surface of the samples are shown in Fig. 4. The sample which has best thermoelectric properties ($(Bi_2Te_3)_{0.15}(Sb_2Te_3)_{0.85}$) shows laminar structure and better realigned grains as shown in Fig. 4a.

The temperature dependence of electrical conductivity for all samples has been studied. It has been observed that the electrical conductivity increased with increasing temperature, which indicates that the microstructured alloys have semiconducting behavior. It was also found that the electrical conductivity (σ) increased with increase of the Sb content. For instance, electrical conductivity (σ) increased from about 5.9×10^4 $(\Omega \cdot m)^{-1}$ to 1.28×10^5 $(\Omega \cdot m)^{-1}$ when the Sb content is increased from $x = 0.15$ to $x = 0.3$ at 300 K.

The semiconductors show activated temperature dependence according to the relation (3).

$$\sigma = \sigma_0 \exp(-\Delta E/k_B T) \quad (3)$$

where ΔE and σ_0 are the activation energy and pre-exponential factor respectively. Fig. 5 shows temperature dependence of dc conductivity for (4)

$$n_\sigma = 2(2\pi m k_B T/h^2)^{2/3} \exp(-\Delta E/k_B T) \quad (4)$$

where m is the mass of charge carrier and k_B is the Boltzmann constant.

Electrical conductivity can be expressed in terms of the carrier concentration (n), as follows:

$$\sigma = ne\mu \quad (5)$$

where μ is the carrier mobility, e is the electron charge and n is the carrier concentration**.** It was found that the free charge carrier concentration (n_σ) and electrical conductivity (σ) increased with increasing Sb content. Previous studies [25, 27-28], indicate the holes are generally created by the antistructure defects resulted from substituting Te atoms by Bi and Sb in the p-type $(Bi_2Te_3)_x(Sb_2Te_3)_{1-x}$ ($x = 0.15$, 0.2, 0.25 and 0.3) alloys. A decrease of difference in electronegtivity between the component atoms ($\chi_{Sb} = 2.05$, $\chi_{Bi} = 2.02$ and $\chi_{Te} = 2.1$) will be favorable to form the antistructure defects. Hence, the carrier (hole) concentration and electrical conductivity increased with increasing Sb content because more antistructure defects are formed due to small difference in electronegtivity between Sb and Te than that between Bi and Te.

The total thermal conductivity consists of a phononic contribution k_l and a contribution of mobile charge carriers, k_c, i.e. $k_{total} = k_l + k_c$. Usually, the carrier thermal conductivity (k_c) can be estimated by the Wiedemann-Franz law, which relates k_c to the electrical conductivity (σ) according to $k_c = L_0 T\sigma$, where Lorenz number is taken to be $L_0 = 2.45 \times 10^{-8}$ V^2/K^2. It can be seen from Table 2, the carrier thermal conductivity (k_c) increased with increasing Sb content from $x = 0.15$ to 0.3, which is originated from the increase in electrical conductivity due to increase in carrier concentration.

The positive value of the Seebeck coefficient for $(Bi_2Te_3)_x(Sb_2Te_3)_{1-x}$ ($x = 0.15$, 0.2, 0.25 and 0.3) determined over the temperature ranging from 298 K to 465 K, as shown in Fig. 6, means that the major charge carriers in all the samples are holes. The Seebeck coefficient for $(Bi_2Te_3)_x(Sb_2Te_3)_{1-x}$ samples was observed to

Table 2 – Carrier type concentration, electrical conductivity (σ), activation energy (ΔE), free charge carrier concentration (n_σ), total thermal conductivity(k_{total}), carrier thermal conductivity (k_c), Seebeck coefficient (α), power factor (PF) and dimensionless figure of merit (ZT) for $(Bi_2Te_3)_x(Sb_2Te_3)_{1-x}$($x = 0.15$, 0.2, 0.25 and 0.3) alloys at 300 K

Material	Type	$\sigma \times 10^5$ $(\Omega \cdot m)^{-1}$	ΔE (eV)	$n_\sigma \times 10^{19}$ (cm^{-3})	k_{total} (W/m·K)	k_c (W/m·K)	α (μV/K)	PF $\times 10^{-3}$ $(Wm^{-1}K^{-2})$	ZT
$(Bi_2Te_3)_{0.3}(Sb_2Te_3)_{0.7}$	p	0.591	0.02	1.15	1.18	0.43	+ 195	2.3	0.57
$(Bi_2Te_3)_{0.25}(Sb_2Te_3)_{0.75}$	p	0.734	0.018	1.23	1.22	0.53	+ 182	2.4	0.59
$(Bi_2Te_3)_{0.2}(Sb_2Te_3)_{0.8}$	p	0.942	0.017	1.29	1.26	0.68	+ 175	2.8	0.68
$(Bi_2Te_3)_{0.15}(Sb_2Te_3)_{0.85}$	p	1.28	0.014	1.45	1.32	0.94	+ 158	3.2	0.72

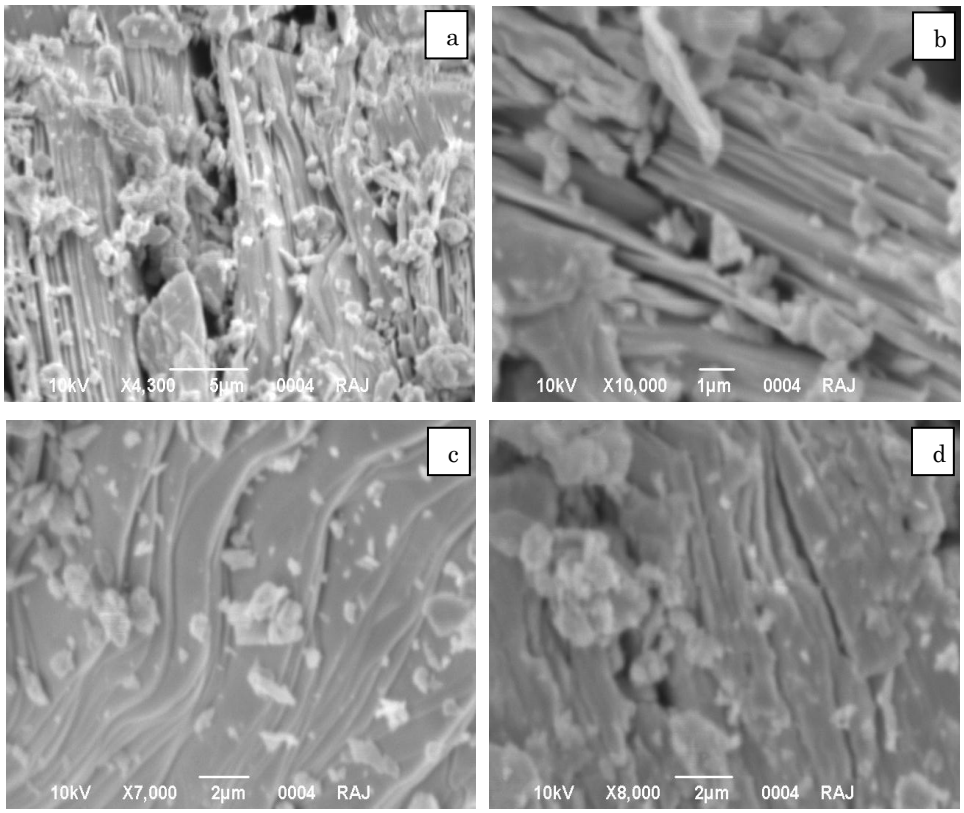

Fig. 4 – SEM micrograph of $(Bi_2Te_3)_{0.15}(Sb_2Te_3)_{0.85}$ (a), $(Bi_2Te_3)_{0.2}(Sb_2Te_3)_{0.8}$ (b), $(Bi_2Te_3)_{0.25}(Sb_2Te_3)_{0.75}$ (c), $(Bi_2Te_3)_{0.3}(Sb_2Te_3)_{0.7}$ (d)

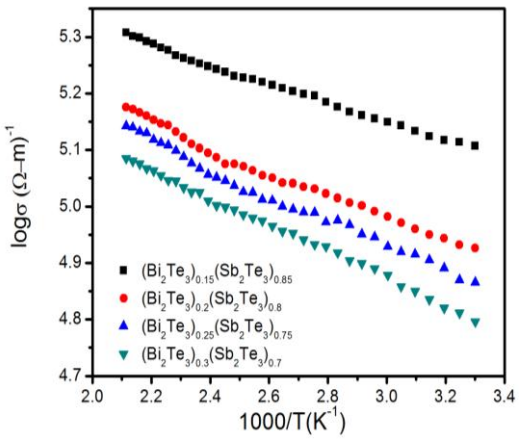

Fig. 5 – Temperature dependence of the dc conductivity of $(Bi_2Te_3)_x(Sb_2Te_3)_{1-x}$ (x = 0.15, 0.2, 0.25 and 0.3) alloys

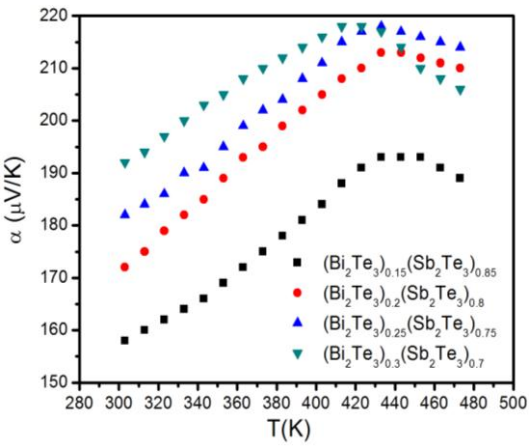

Fig. 6 – Temperature dependence of the Seebeck coefficient of $(Bi_2Te_3)_x(Sb_2Te_3)_{1-x}$ (x = 0.15, 0.2, 0.25 and 0.3) alloys

increase with increasing temperature, and after reaching a maximum value, it showed a slight decrease with further increase in temperature which is due to excitation of carriers at higher temperature. This type of behavior also has been reported previously [29]. The Seebeck coefficient strongly depends on carrier concentration and can be expressed as follow:

$$\alpha = \left(8\pi^2 k_B^2 / 3eh^2\right) m^* T \left(\pi/3n\right)^{2/3} \qquad (6)$$

where e is the electron charge, m^* is the effective mass, h is the Planck constant and μ is the carrier mobility. The Seebeck coefficient at 300 K decreased from about + 195 μV/K to + 158 μV/K by increasing the Sb content from x = 0.7 to 0.85 due to increase in carrier concentration.

The temperature dependence of power factor for $(Bi_2Te_3)_x(Sb_2Te_3)_{1-x}$ is shown in Fig. 7. It is well known that optimizing the power factor PF = $\alpha^2\sigma$ of a thermoelectric material always involves a compromise on the Seebeck coefficient (α) and on the electrical conductivity (σ). Here we observed that the Seebeck coefficient first increases and then shows a slight decrease with increase in temperature. Also electrical conductivity of semiconductors increases with increase of temperature. The power factor of $(Bi_2Te_3)_x(Sb_2Te_3)_{1-x}$ first increases with increasing temperature and at a certain temperature becomes a constant value which is due to dependence of power factor on the Seebeck coefficient and on the electrical conductivity.

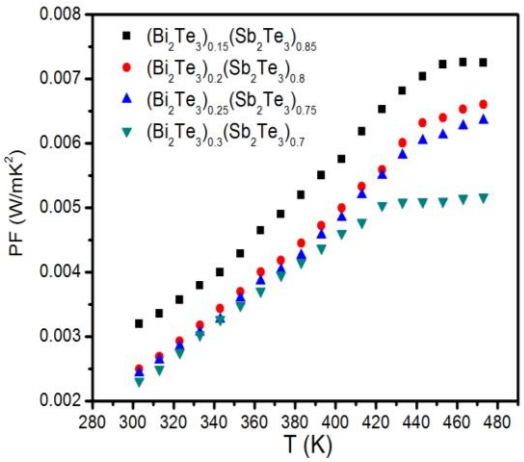

Fig. 7 – Temperature dependence of the power factor of $(Bi_2Te_3)_x(Sb_2Te_3)_{1-x}$ (x = 0.15, 0.2, 0.25 and 0.3) alloys

At 300 K, the calculated values of figure-of-merit ($ZT = \sigma\alpha^2 T/\kappa$) are shown in Table 2. It is evident from Table 2 that the sample corresponding to the composition of 15 %Bi_2Te_3–85 %Sb_2Te_3 has the best thermoelectric properties.

4. CONCLUSIONS

The microstructured $(Bi_2Te_3)_x(Sb_2Te_3)_{1-x}$ alloys with various chemical composition (x = 0.15, 0.2, 0.25 and 0.3) have shown p-type conduction. The influence of the variations of Sb content on the optical and thermoelectric properties has been studied. The optical band gap decreased with increase of the Sb content and result indicated the significant band gap shrinkage at higher doping levels. The SEM micrographs provide that the sample which has best thermoelectric properties show laminar structure and better realigned grains. Also, the results show that the increase in Sb content caused decrease in Seebeck coefficient and increase in electrical conductivity and thermal conductivity due to increase in hole concentration. As a result, at 300 K, the maximum figure of merit (ZT) of 0.72 has been obtained for the composition of 15 %Bi_2Te_3–85 %Sb_2Te_3.

AKNOWLEDGEMENTS

The authors are thankful to Dr. S.K. Tripathi for his support and guidance and highly grateful to National Physics Laboratory (NPL), New Delhi and Panjab University, Chandigarh for providing research facilities.

REFERENCES

1. L. Weiling, Tu. Shantung, *Chin. Sci. Bull.* **49**, 1212 (2004).
2. K.H. Lee, O.J. Kim, *Int. J. Heat Mass Transfer* **50**, 1982 (2007).
3. J.S. Zhang, W.L. Luan, H. Huang, Y.S. Qi, S.T. Tu, *Sensor. Actuat. B* **128**, 266 (2007).
4. M. Alkhalfioui, A. Michez, A. Giani, A. Boyer, A. Foucaran, *Sensor. Actuat. A* **107**, 36 (2003).
5. A.W. Ruff, K.G. Kreider, *Wear* **187**, 203 (1997).
6. B. Sorli, F. Delannoy, A. Giani, A. Foucaran, A. Boyer, *Sensor. Actuat. A* **100**, 24 (2002).
7. E. Socher, O. Degani, Y. Nemirovsky, *Sensor. Actuat. A* **71**, 107 (1998).
8. H. Huang, L. Wei-Ling, T. Shan-Tung, *Thin Solid Films* **517**, 3731 (2009).
9. X.B. Zhao, X.H. Ji, Y.H. Zhang, T.J. Zhu, J.P. Tu, X.B. Zhang, *Appl. Phy. Lett.* **86**, 062111 (2005).
10. G.A. Slack, V.G. Tsoukala, *J. Appl. Phys.***76**, 1665 (1994**)**.
11. T.M. Tritt, *Science* **283**, 804 (1999).
12. B.C. Sales, D. Mandrus, R.K. Williams, *Science* **272**, 1325 (1996).
13. G.S. Nolas, D.G. Vanderveer, A.P. Wilkinson, J.L. Cohn, *J. Appl. Phys.* **91**, 8970 (2002).
14. D.X. Huo, T. Sasakawa, Y. Muro, T. Takabatake, *Appl. Phys. Lett.* **82**, 2640 (2003).
15. Y.M. Lin, O. Rabin, S.B. Cronin, J.Y. Ying, M.S. Dresselhaus, *Appl. Phys. Lett.* **81**, 2403 (2002).
16. M.S. Sander, A.L. Prieto, R. Gronsky, T. Sands, A.M. Stacy, *Adv. Mater.* **14**, 665 (2002).
17. R. Venkatasubramanian, E. Siivola, T. Colpitts, B.O. Quin, *Nature* **413**, 597 (2001).
18. L.D. Hicks, T.C. Harman, M.S.E. Dresselhaus, *Appl. Phys. Lett.* **63**, 3230 (1993).
19. W. Wang, F.L. Jia, Q.H. Huang, J.Z. Zhang, *Microelectron. Eng.* **77**, 223 (2005).
20. O. Yamashita, H. Odahara, *Appl. Phys.* A **85**, 45 (2006).
21. C. Zhao, F. Ping, Z. Zhuang, L. Peng, C. Tian, C. Xing, L. Jing, L. Guang, Z. Dong, *Appl. Surf. Sci.* **280**, 225 (2013).
22. W.J. Xie, X.F. Tang, Y.G. Yan, Q.J. Zhang, T.M. Tritt, *J. Appl. Phys.* **105**, 113713 (2009).
23. J. Jiang, L. Chen, S. Bai, Q. Yao, Q. Wang, *J. Cryst Growth* **277**, 258 (2005).
24. C. Euvananout, N. Jantaping, C. Thanachayanont, *Curr. Appl. Phys.* **11**, 246 (2011).
25. D. Li, R.R. Sun, X.Y. Qin, *Intermetallics* **19**, 2002 (2011).
26. G. Xianhui, Y. Junyou, Z. Wen, H. Jie, B. Siqian, F. Xian, D. Xingkai, *Sci. China Ser. E* **49**, 685 (2006).
27. J. Horak, K. Cermak, L. Koudelka, *Phys. J. Chem. Solids* **47**, 805 (1986).
28. V.A. Kulbachinskii, A.Yu. Kaminskii, V.G. Kytin, P. Lostakb, Drasar, A. de Visser, *J. Exp. Theor. Phy.* **90**, 1081 (2000).
29. D.H. Kim, C. Kim, S.H. Heo, H. Kim, *Acta Mater.* **59**, 405 (2011).
30. Z.H. Khan, M. Zulefquar, M. Ilyas, M. Husain, *Acta Phys. Pol.* A **98**, 93 (2000).
31. L.M. Goncalves, C. Couto, P. Slpuim, D.M. Rowe, J.H. Correia, *Mater. Sci. Forum* **514-516**, 156 (2006).
32. J. Horak, K. Cermak, L. Koudelka, *Phys. J. Chem. Solids* **47**, 805 (1986).
33. F.J.Di. Salvo, *Science* **285**, 703 (1999).
34. K. Satou, O. Yamashita, H. Odahara, S. Tomiyoshi, *Appl. Phys. A* **84**, 103 (2006).
35. P.P. Pradyumnan, S. Krishnan, *Ind. J. Pure Appl. Phys.* **48**, 115 (2010).
36. O.V. Galan, F.C. Gandarilla, J. Fandino, F. Roy, J.S. Hernandez, G.C. Puente, *Semicond. Sci. Technol.* **24**, 025025 (2009).
37. L.M. Goncalves, C. Couto, P. Alpuim, D.M. Rowe, J.H. Correia, *Sensor. Actuat. A* **130**, 346 (2006).
38. S.K. Pundir, S. Singh, A.K. Srivastava, M.K. Dalaiand, R. Kumar, *Adv. Sci. Eng. Med.* **5**, 436 (2013).
39. H. Zou, D.M. Rowe, S.G.K. Williams, *Thin Solid Films* **408**, 270 (2002).
40. H. Bottner, J. Nurnus, A. Gavrikov, G. Kuhner, M. Jagle, C. Kunzel, D. Eberhard, G. Plescher, A. Schubert, K.H. Schlereth, *J. Microelectromech. Syst.* **13**, 414 (2004).

41. Z. Stary, J. Horak, M. Stordeur, M. Stolzer, *Phys. J. Chem. Solids* **29**, 49 (1988).
42. C.Z. kun Cai, F. Ping, Z. Zhuang, L. Peng, C. Tian, C. Xing, L. Jing, L. Guang, Z. Dong, *Appl. Surf. Sci.* **280**, 225 (2013).
43. H. Zou, D.M. Rowe, G. Min, *J. Vac. Sci. Technol.* A **19**, 899 (2001).
44. P. Srivastava, K. Singh, *Mater. Lett.* **75**, 42 (2012).
45. D.L. Medlin, G.J. Snyder, *Curr. Opin. Colloid Interface Sci.* **14**, 226 (2009).
46. P. Srivastava, K. Singh, *Therm. Anal. Calorim.* **110**, 523 (2012).
47. J. Dheepa, R. Sathyamoorthy, A. Subbarayan, *J. Cryst. Growth* **274**, 100 (2005).
48. W.H. Chao, W.C. Lei, Z.J. Liang, Z.M. Lei, L. Jian, S.W. Bin, Y. Na, M.L. Mo, *Chin. Phys. Lett.* 26, 107301 (2009).